Escherichia coli Bacteria-Templated Synthesis of Nanoporous Cadmium Sulfide Hollow Microrods for Efficient Photocatalytic Hydrogen Production

Liming Shen,[†] Ningzhong Bao,*[,†] Peter E. Prevelige,[‡] and Arunava Gupta*[,†]

Centre for Materials for Information Technology, University of Alabama, Tuscaloosa, Alabama 35487, Department of Microbiology, University of Alabama at Birmingham, Birmingham, Alabama 35294

Received: November 14, 2009; Revised Manuscript Received: January 4, 2010

A simple sonochemical method has been utilized to synthesize nanoporous hollow structures of semiconducting cadmium sulfide (CdS) using *Escherichia coli* bacteria as template. To enable adsorption and reaction throughout the *E. coli* cell envelope, the cell permeability is enhanced by suitable ethanol treatment while preserving the morphology. With cadmium acetate and thioacetamide as reactants, CdS nanostructures in the form of monodisperse quantum dots, nearly monodisperse nanocrystals, and nanoporous hollow microrods are controllably formed on ethanol-treated *E. coli* with increasing reaction time. Additionally, nanorod antennas have been fabricated by utilizing the pili formed during the growth phase of the bacteria. The CdS crystal structure can be tuned from being pure cubic to a mixture of cubic and hexagonal or pure hexagonal by simply adjusting the sulfur/cadmium molar ratio of the reactants. Photoanodes fabricated using the hexagonal structured CdS nanoporous hollow microrods exhibit excellent performance for photocatalytic hydrogen production, with a maximum photoelectrochemical cell efficiency of 4.3% under global AM 1.5 illumination. This is significantly better than the 1.2% efficiency obtained using CdS nanoparticles synthesized utilizing the same procedure in the absence of *E. coli*. The bacterial template route has been extended to the synthesis and assembly of other chalcogenide nanostructures, including PbS, HgS, and ZnS. Use of chalcogenide hollow nanostructures with mixed stoichiometry can potentially lead to further improvements in the photoconversion efficiency.

Introduction

Sulfides, such as CdS,[1] $AgInS_2$,[2] $CuInS_2$,[3,4] etc., are a group of narrow-band-gap semiconductors that have been widely researched as candidates for visible-light-driven photocatalysis. In the presence of a sacrificial reagent and with a band gap of about 2.4 eV and a flat-band potential at −0.66 V (pH 7), CdS is an excellent photocatalyst for H_2 production under visible light irradiation.[5,6] It should be noted that the band gap structure of the material is only a thermodynamic requirement and not a sufficient condition for efficient photocatalysis. The solar energy conversion efficiency of a photocatalyst is strongly dependent on materials-related characteristics, including crystal structure, crystallinity, particle size, and distinctive nanostructures.[7] These factors directly influence the band gap structure and electron transfer processes, including charge separation, transport of the photogenerated carriers, and photochemical reactivity at the photocatalyst/electrolyte interface. Cadmium sulfide nanocrystals with the hexagonal crystal structure have shown photocatalytic activity that is superior to the pure cubic or a mixture of cubic and hexagonal phases.[6] Recent studies indicate that nanoporous hollow structures provide a shorter pathway for the transfer of excited electrons in semiconductors.[8,9] Accordingly, nanoporous hexagonal CdS with a hollow structure, prepared using a two-step chemical reaction, exhibits high activity (quantum yield = 60.34%) for photocatalytic hydrogen production under visible light irradiation ($\lambda \geq 420$ nm).[10]

Hollow structures have, in fact, attracted attention for a variety of applications and are commonly fabricated on presynthesized templates, such as polystyrene,[11,12] silica spheres,[13,14] etc. In recent years, a wide range of microbiological organisms, including proteins,[15,16] nucleic aids,[17,18] phage,[19] bacteria,[20] and complex multicellular systems,[21] have also been investigated as templates. Using such biological systems, a number of inorganic nanomaterials have been synthesized with precisely controlled size, shape, structure, and functionality.[22−25] These nanomaterials can be further assembled into more complex functional structures and devices.[26,27] From a practical viewpoint, unicellular microorganisms, such as bacteria, are attractive templates for materials synthesis since they are readily available in a wide variety of shapes and sizes, and a number of them are environmentally benign and can be readily amplified under ambient conditions.[28]

Bacterial systems, including *Clostridium*, *Klebsiella aerogenes*, and *Escherichia coli* (*E. coli*), have been used to biosynthesize CdS nanocrystals.[29] *E. coli* is of particular interest, since it is a Gram-negative bacteria and is by far the most well-studied bacterial system. The genetic tools and cellular metabolisms associated with this bacterium are fairly well understood. *E. coli* is also one of the longest rod-shaped bacteria.[30] Using *E. coli*, intracellular hexagonal CdS nanocrystals have been produced with a size distribution of 2−5 nm when the bacteria are incubated in a solution containing cadmium chloride and sodium sulfide.[31] The nanocrystal yield varies dramatically, depending on the growth phase of the cells; increasing nearly 20-fold in *E. coli* cells grown to the stationary phase, as compared with those grown to the late logarithmic phase. More recently, the microbial synthesis of CdS nanocrystals in genetically engineered *E. coli*, produced by expressing the phytochelatins synthase of *Schizosaccharomyces pombe* (SpPCS), has

* Corresponding author. E-mail: nzhbao@mint.ua.edu; agupta@mint.ua.edu.
[†] University of Alabama.
[‡] University of Alabama at Birmingham.

10.1021/jp910842f
Published on Web 01/26/2010

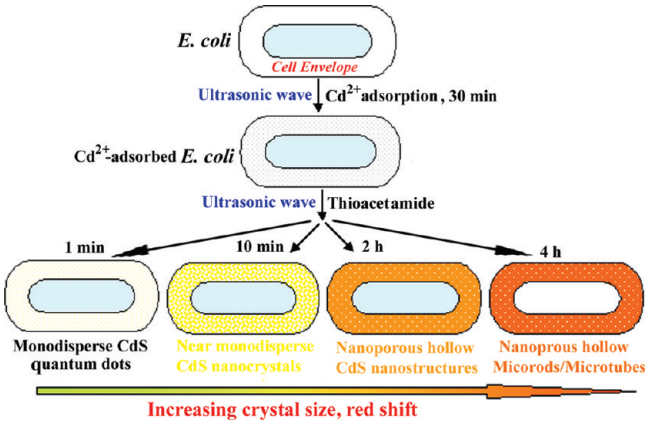

Figure 1. A schematic diagram illustrating the concept of *E. coli*-templated synthesis and assembly of nanoporous hollow CdS nanostructures.

been reported.[32] By controlling the population of the capping PCs, *E. coli* cells have been engineered as an ecofriendly biofactory to produce uniformly sized, PC-coated CdS nanocrystals. In both reported cases, the intracellularly synthesized CdS in the form of nanocrystals has to be collected by disrupting the cells. Furthermore, the concentrations of the inorganic reactant salts have to be carefully controlled to avoid rapid, uncontrolled precipitation of CdS particles in solution. Thus far, the controllable intracellular synthesis and assembly of more complex CdS architectures on *E. coli* has not been feasible because the low permeability of cell envelope and efflux pump inhibition[33,34] of the bacteria prevents nucleation of the inorganic throughout the cell envelope.

We have developed a simple sonochemical route for the synthesis and assembly of CdS nanostructure with high yield under mild ambient conditions by exploiting the chemical characteristics and structure of permeabilized *E. coli* bacteria. Although other bacteria such as *Lactobacillus bulgaricus* have been used as a template to prepare ZnS on the cell surface by combining sonochemistry,[35] the novelty of the present method lies in the use and modification of *E. coli* for the templating growth of CdS with controllable materials properties.

E. coli is one of the most extensively studied bacterial systems. It is a Gram-negative bacterium and is also one of the longest rod-shaped bacteria.[30] Motivated by its use in Gram staining, we have developed an ethanol treatment method to enhance the permeability of *E. coli* while retaining the morphology.[36] The role of ethanol is to dissolve the lipid layer of the outer membrane, thus enabling Cd^{2+} adsorption and reaction throughout the cell envelope. On addition of thioacetamide, H_2S is gradually produced by sonochemical decomposition,[37] which then reacts rapidly with the adsorbed cadmium ions to nucleate and grow CdS throughout the cell envelope. With increasing reaction time, the CdS nanoparticles grow larger and coalesce to form continuous hollow nanostructures. Thus, by simply changing the reaction time, CdS nanostructures in the form of monodisperse quantum dots, nearly monodisperse nanocrystals, and nanoporous hollow microrods are controllably formed throughout the whole cell envelope of the *E. coli* using cadmium acetate and thioacetamide as reactants. The process is schematically illustrated in Figure 1. As expected, the synthesized CdS show a distinct red shift with increasing size of the nanostructures. We have also fabricated novel structures consisting of CdS nanorod antennas attached to nanoporous hollow microrods by using the *E. coli* pili as templates. In addition to varying the morphology, we can precisely control the crystal phase of CdS products from cubic, a mixture of cubic and hexagonal, to pure hexagonal by merely adjusting the sulfur/cadmium molar ratio of the reactants. Photoanodes fabricated using the hexagonal structure CdS nanoporous hollow microrods exhibit excellent performance for photocatalytic hydrogen production, with a maximum photoelectrochemical cell efficiency of 4.3% under global AM 1.5 illumination. We have extended the bacterial synthesis approach to the synthesis and assembly of other sulfides, including PbS, ZnS, and HgS.

Experimental Section

Preparation of Cells. *E. coli* strain ER2738 was supplied by New England Biolab. The ER2738 cells were incubated in LB medium overnight, centrifuged at 10 000 rpm for 10 min, and then resuspended in 1/7 volume sterile deionized water (the concentration of cells was $\sim 10^9$ CFU/mL). One milliliter of this cell culture was centrifuged, and the cell pellet was completely dispersed in 95% ethanol for 3 min, followed by the addition of 50 mL of sterile deionized water. Ethanol-treated ER2738 cells were collected by centrifugation and then resuspended in 50 mL of sterile deionized water for the CdS synthesis reaction.

Synthesis of CdS Nanostructures. Cadmium acetate dihydrate and thioacetamide were purchased from Acros Organics and used as received. In a typical procedure, 0.5 mmol of cadmium acetate dehydrate was first added to 50 mL of ethanol-treated ER2738 solution, and 0.5 mmol of thioacetamide was subsequently added after 30 min. The reactions were conducted for up to 4 h in an ultrasonic bath with the temperature maintained at around 28 °C. The resulting solutions were used to prepare samples for characterization. The time-dependence of the size, shape, and structure of the *E. coli*-templated CdS structures were investigated by varying the reaction time. By adjusting the sulfur/cadmium molar ratio, the crystal phase of the CdS product could be precisely controlled from cubic, a mixture of cubic and hexagonal, to pure hexagonal. For example, to supply more sulfide ions in a short time for decreasing the Cd/S ratio, the thioacetamide concentration was increased so that a suitable amount of hydrogen sulfide could be produced rapidly. The synthetic procedure has been extended to the synthesis of a variety of other sulfides such as PbS, HgS, and ZnS.

Characterization of Materials. The morphology and structure of the CdS products were investigated using a combination of scanning electron microscopy (SEM, Philips X-30), operating at 20 kV, and transmission electron microscopy (TEM, coupled with high resolution (HR), Tecnai F-20), operating at 200 kV. The composition was carried out using energy dispersive X-ray spectroscopy (EDS), equipped on the SEM. X-ray diffraction (XRD) patterns of samples were obtained on a Bruker D8 Advance X-ray diffractometer (Co irradiation, $\lambda = 1.7889$ Å), in the continuous scan mode over 20−70° (2θ) with a scanning rate of 0.02° (2θ)/s, operating at 45 kV and 20 mA. The UV−visible (UV−vis) absorption spectrum of all the samples dispersed in water was recorded using a Varian Cary UV−vis spectrophotometer.

Photoelectrochemical Characterization. The photoanode was fabricated by spin-coating several layers of 0.05 g/mL *E. coli*-templated CdS ethanol solution onto an ITO-coated glass substrate (1 cm × 1 cm) and was then annealed at 300 °C in high-purity N_2 for 0.5 h. The *E. coli*-templated CdS used for fabrication of the electrode was synthesized by the typical synthetic procedure described above. For comparison, photoanode consisting of an identical amount of CdS nanoparticles

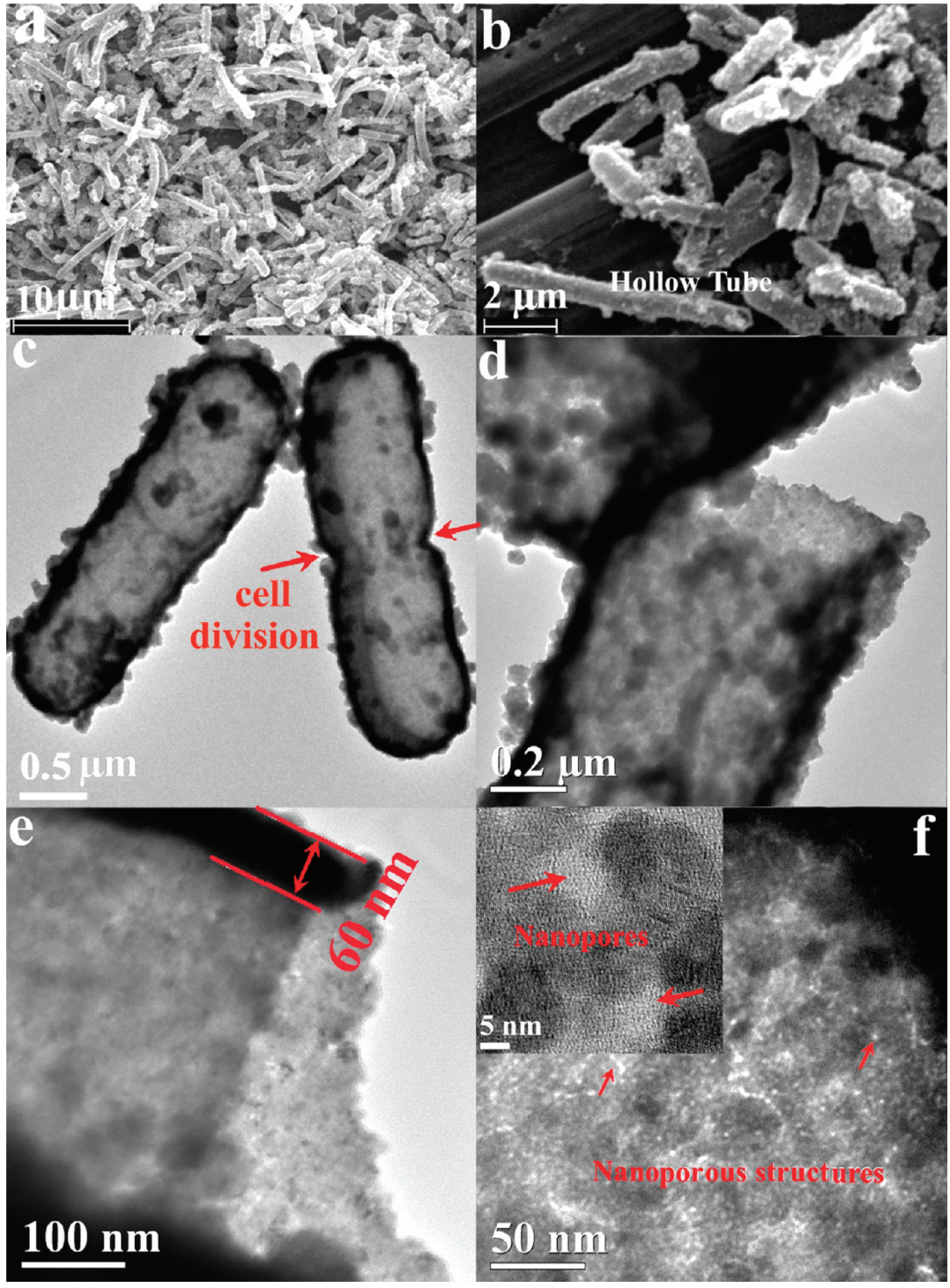

Figure 2. SEM and TEM images of *E. coli*-templated nanoporous hollow CdS microrods formed after 4 h. (a) Low-magnification and (b) high-magnification SEM images of the hollow structures showing the high yield of product with the desired shape. TEM image of hollow CdS microrods with (c) closed ends, and (d) an open end. The magnified TEM images of (e) the cross section and (f) the body of a rod-like hollow CdS structure show the uniform wall thickness and the nanoporous structure of the wall, respectively.

synthesized in the absence of *E. coli* template was fabricated using the same procedure. An EG&G potentiostat was used to measure the photoelectrochemical response of the fabricated photoanodes with a conventional three-electrode system consisting of a Ag/AgCl reference electrode and a Pt foil counter electrode. A 1 M Na_2S/0.5 M $NaSO_3$ aqueous solution was used as the electrolyte. A solar simulator with an illumination intensity of one sun (AM 1.5, 100 mW/cm^2, Newport Corporation) was used as the light source. A power meter (Scientech, Inc.) was used to calibrate the input power before and after the photoelectrochemical measurements. The photoelectrochemical cell efficiency was used as the parameter to evaluate the photoelectrochemical property of the synthesized materials.[38,39]

Results and Discussion

The composition, crystal phase, morphology, structure, and optical absorption properties of the products have been examined using EDS, XRD, SEM, (HR) TEM, and UV−vis spectroscopy. Figure 2 shows the typical morphology and structure of as-

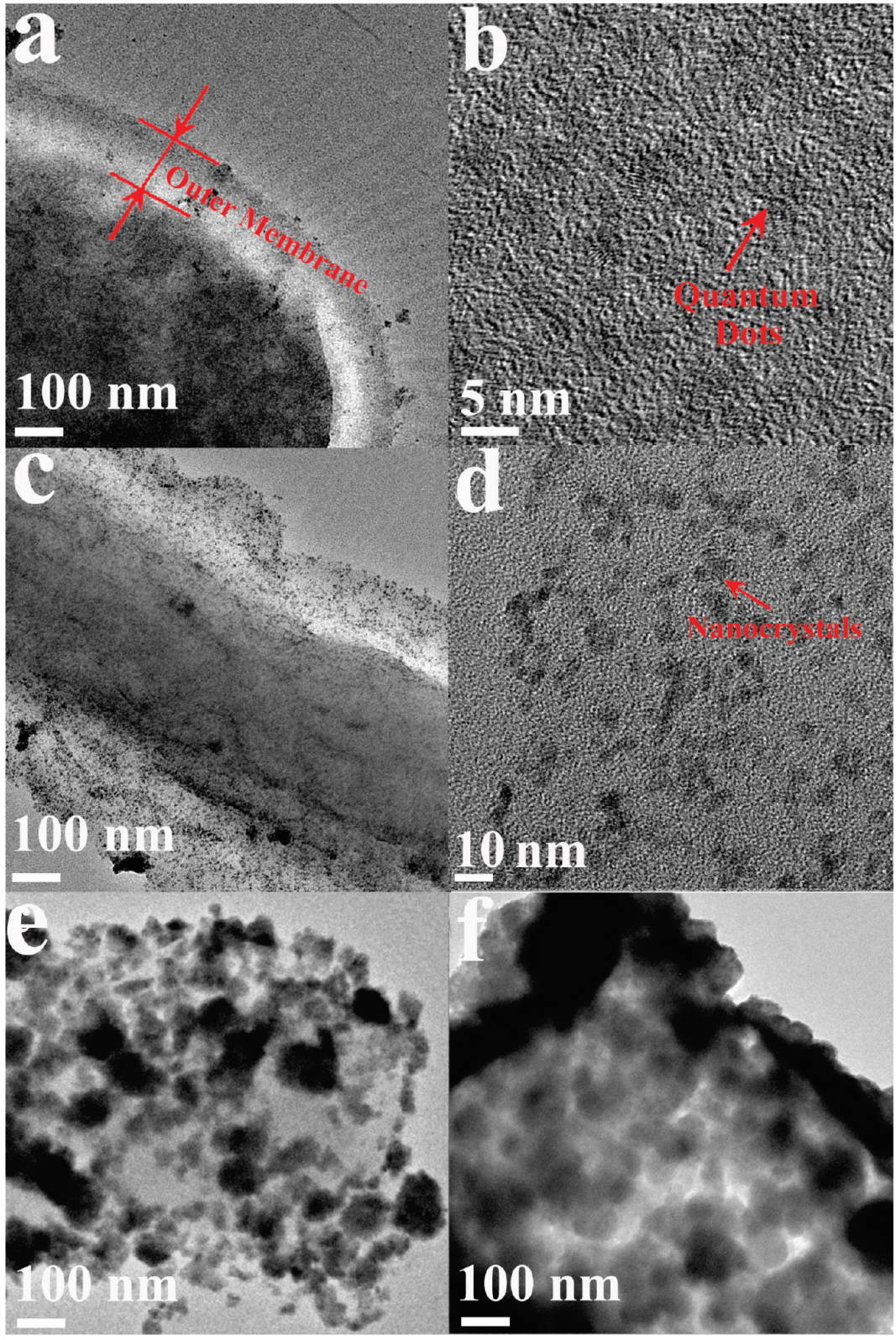

Figure 3. TEM and HRTEM images of synthesized CdS nanomaterials as a function of reaction time. (a, b) Monodisperse quantum dots formed after 1 min; (c, d) nearly monodisperse nanocrystals formed after 10 min; (e) continuous nanoparticle agglomerates formed after 2 h; and (f) uniform porous coating formed after 4 h.

synthesized *E. coli*-templated nanoporous hollow CdS microrods obtained after a reaction time of 4 h. Figure 2a and b show the large-area and magnified SEM images of the products, respectively. The shape and dimension of most of the product is very close to that of *E. coli*, being rodlike with around 2.5 μm length and 0.8 μm diameter, which indicates that the bacterium indeed acts as a template for the synthesis. A small fraction of the product has a longer length and some exhibit open-ended structures, as seen in Figure 2b and d. The latter is caused by cell division, which is a natural process during cell growth. The CdS microrod imaged on the right in Figure 2c is formed at the start of cell division, as suggested by the narrowed diameter

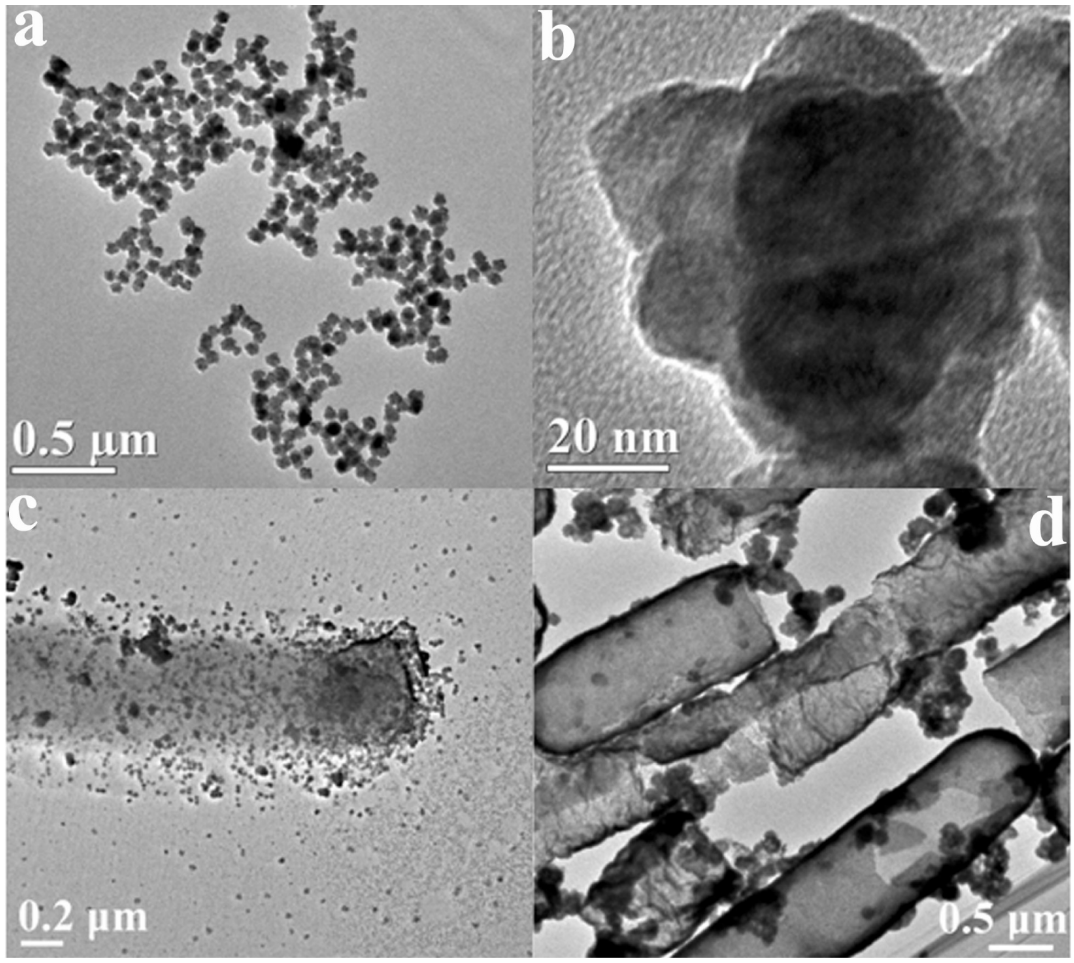

Figure 4. TEM images of (a, b) crystalline CdS nanoparticles sonochemically synthesized after 4 h in the absence of *E. coli* bacteria, and CdS nanoparticles formed in the reaction solution and on the cell surface of untreated *E. coli* bacteria after (c) 1 min and (d) 2 h.

in the mid section that appears pinched, whereas the microrod imaged in the left has a uniform diameter over the entire length, since it forms before cell division. The TEM cross section image for products formed at the time of cell division have an open end, as observed in Figure 2d.

The hollow nature of the CdS microrods is quite apparent, based on examination of these open-end structures. Figure 2e shows the cross section TEM image of an open-end, hollow microrod. The front and the back sides of the microrod can be readily distinguished by comparing the bright/dark contrast. Since the diameter of the hollow microtubes is around 0.8 μm, it is difficult to image them with both the front and back ends in focus. In Figure 2e, the bright part represents the back side of the microrod, which is in focus, showing the inner surface and structure. The dark part represents the front side of the microrod, showing an unfocused image of the outer surface and structure. From measurement of the dark edge of the microrod in Figure 2e, the wall thickness is estimated to be around 60 nm. The hollow microrods are composed of CdS nanoparticle agglomerates that form a nanoporous structure with uniformly distributed nanopores of around 5 nm in diameter across the entire length. Both nanopores and clear crystal lattice fringes are observed in the HRTEM image shown in the inset to Figure 2f. We have further verified using EDS that the chemical composition of the products is close to stoichiometric with a Cd/S atomic ratio of 1.02.

We have investigated the nucleation and growth of CdS on the ethanol-treated *E. coli* by withdrawing a small amount of the sample from the solution after 1 min, 10 min, 2 h, and 4 h of reaction for TEM imaging and optical absorption measurements. Figure 3 shows the morphology of products formed after 1 min (Figure 3a and b), 10 min (Figure 3c and d), 2 h (Figure 3e), and 4 h (Figure 3f). As seen in Figure 3b, monodisperse single-crystalline CdS quantum dots with dimensions <2.5 nm (over 90% of the nanoparticles have sizes in the range of 2.3 $\pm$ 0.4 nm) are formed inside the cell envelope after 1 min reaction. By prolonging the reaction time to 10 min, the quantum dots grow larger, forming CdS nanocrystals with dimensions <6.5 nm (over 80% of the nanoparticles have sizes in the range of 5.3 $\pm$ 0.5 nm), as seen in Figure 3d. With further increasing the reaction time to 2 h, continuous CdS nanoparticle agglomerates form inside the cell envelope (Figure 3e). The hollow nature of the structure is clearly apparent in the micrograph. After the longest reaction period (4 h), both the density and thickness of the CdS nanoparticle agglomerate increase (Figure 3f), resulting in a uniform porous coating.

To confirm the essential role of *E. coli* as template, we have verified that only CdS nanoparticles of around 80 nm diameter are produced in their absence, under otherwise identical reaction conditions, as seen in Figure 4a and b. As mentioned earlier, the ethanol treatment enhances the cell permeability of *E. coli* to enable Cd^{2+} adsorption and reaction throughout the cell envelope. Thereby, CdS nanostructures in the form of monodisperse quantum dots, nearly monodisperse nanocrystals, and nanoporous hollow microrods are controllably formed on the cell envelope (Figure 3). In contrast, control experiments using

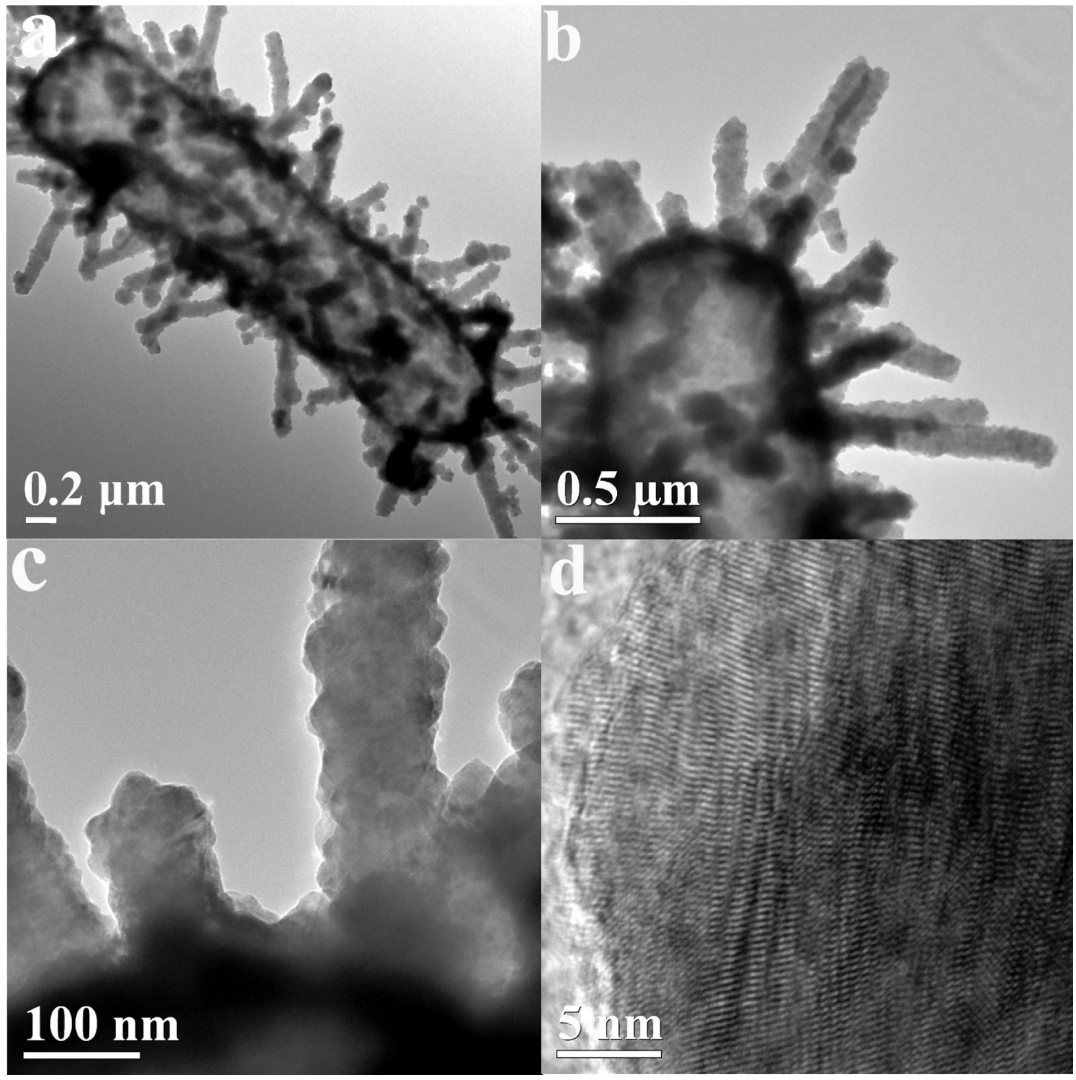

Figure 5. TEM and HRTEM image of nanoporous hollow CdS microrod-supported nanorods synthesized after 4 h using *E. coli* with pili as templates. (a, b) Low-magnification and (c) high-magnification TEM images of the CdS nanostructures show the morphology and structure of the whole CdS assembly, the basic hollow microrod, and the attached nanorods. (d) HRTEM image of the CdS nanorods showing crystal lattice fringes.

untreated *E. coli* as template show formation of CdS nanoparticles both in solution and on the surface of the bacteria after 1 min of reaction (Figure 4c) that then develop into large crystal agglomerates that are nonuniformly distributed on the cell surface after 2 h of reaction (Figure 4d).

An *E. coli* bacterium typically has pili—small hair-like projections emerging from the outside cell surface—during the growth phase. A cell may have from 100 to 300 pili, which are approximately 6.5 nm in diameter and between 200 and 2000 nm in length, with rapid loss of piliation occurring when the culture reaches early stationary phase.[40] We have used the *E. coli* culture grown to the early logarithmic phase ($OD_{600} = 0.5$) as templates after ethanol treatment. The resulting products are nanoporous, hollow CdS microrods with attached CdS nanorod antennas, as seen in Figure 5. The CdS nanorod antennas grow on the pili, with lengths varying from about 200 nm to several micrometers, and a width of around 100 nm. By varying the growth conditions of the *E. coli*, both the number and size of *E. coli*'s pili can to be controlled. Correspondingly, the size, structure, and the density of the CdS nanorod antennas can be manipulated. The HRTEM image shown in Figure 5d indicates good crystallinity of the CdS antennas.

By increasing the reaction time, a gradual transition in the color of the solution from colorless; to nearly colorless; to yellow; to orange; and, finally, to dark orange is observed, as shown in the photographs in Figure 6. Consistent with the TEM images of Figure 3, a distinct red shift is noted in the absorption spectra as a function of reaction time in Figure 6, confirming the increase in size of the CdS nanoparticles formed on the cell envelope. The spectra of the product formed after 4 h (Figure 6e), with a peak at around 520 nm, is similar to that of bulk CdS. As seen in Figure 6e, the absorption edge for the sample obtained after 4 h reaction is at about 550 nm, which is at longer wavelength than the band gap of bulk CdS. This is likely caused by Rayleigh scattering, since the products are nanoporous hollow structures composed of nanoparticles, similar to earlier reported nanostructures.[10] Although the synthesized hollow microrods have a diameter of about 800 nm, the walls of the hollow microrod are composed of uniformly distributed CdS nanoparticle agglomerates consisting of nanoparticles of diameter in the range of 5−15 nm and nanopores of around 5 nm. The dimension of the nanopores is extremely small as compared to the wavelength of UV and visible light (200−800 nm), resulting in the Rayleigh scattering phenomenon.

As mentioned previously, the photocatalytic efficiency of CdS is dependent on its crystalline phase, with the hexagonal variant exhibiting the highest photocatalytic activity for hydrogen production under visible light irradiation.[6,10] Thioacetamide is

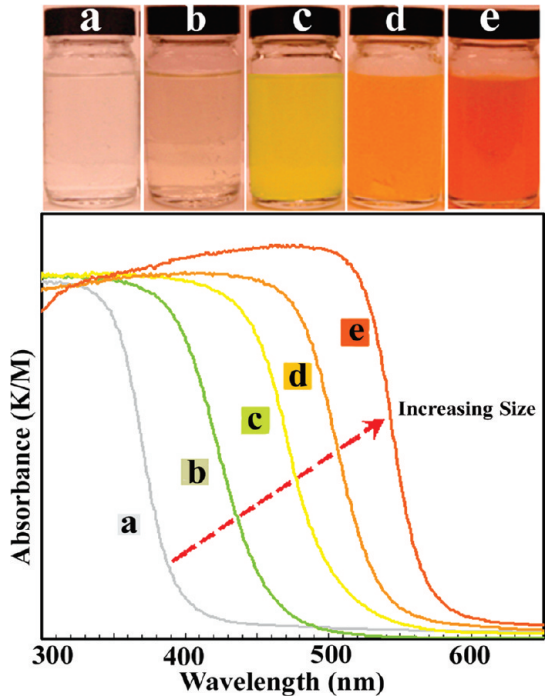

Figure 6. Optical images and UV−vis spectra of *E. coli*-templated CdS nanostructures in solution after (a) 0 min, (b) 1 min, (c) 10 min, (d) 2 h, and (e) 4 h of reaction.

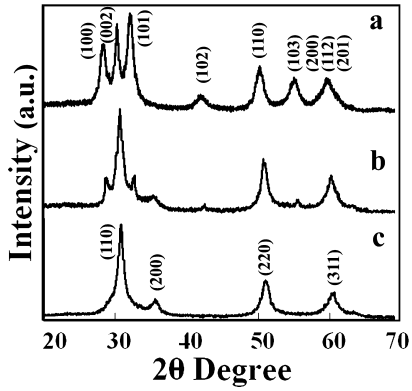

Figure 7. XRD patterns of *E. coli*-templated CdS nanostructures with (a) hexagonal, (b) mixture of hexagonal and cubic CdS nanocrystals, and (c) cubic phase structures, obtained with decreasing sulfur/cadmium molar ratio from 2.5, 1, and 0.25, respectively.

widely used as a sulfur source for the sonochemical synthesis of metal sulfides in the form of films, coatings, etc. because of its slow reaction rate with metal ions.[36,41] In most reported studies, the crystal structure of the material has not been investigated, including the case of bacteria-templated synthesis of CdS. We have achieved precise control of the crystal phase of the hollow CdS microrods by adjusting the relative molar amount of sulfur in the reactant. Figure 7 shows the XRD patterns of three as-prepared microrod samples, with the crystal structure varying from pure hexagonal (Figure 7a, JCPDS card No. 41-1049), to a mixture of hexagonal and cubic (Figure 7b), to pure cubic phase (Figure 7c, JCPDS card No. 10-0454) by decreasing the sulfur/cadmium molar ratio. In general, the CdS precipitation reaction is rapid as long as sulfide ions are present in the solution, since the CdS has a very small K_{sp}. The decomposition rate of thioacetamide is not expected to change under constant process conditions, such as reaction temperature, pH value, and ultrasound power. Thus, for the synthesis at high sulfur/cadmium molar ratio, we can either increase the concentration of thioacetamide so that a suitable amount of hydrogen sulfide is produced quickly or decrease the concentration of Cd^{2+}.

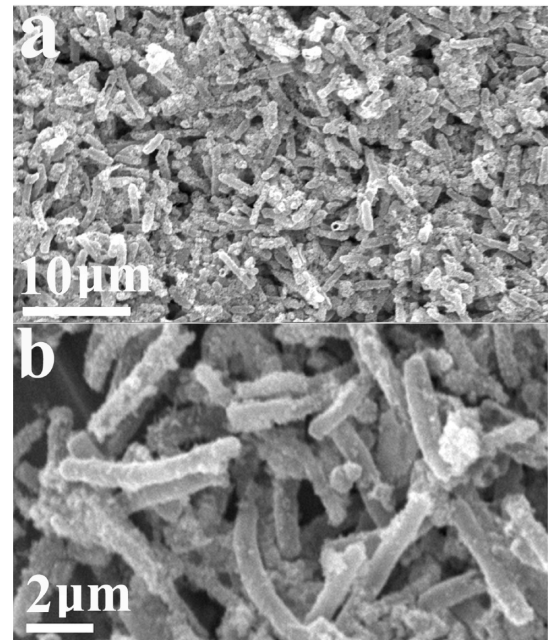

Figure 8. (a) Low- and (b) high-magnification SEM images of *E. coli*-templated hollow CdS microrods after annealing at 300 °C for 0.5 h.

The crystal structure of the product depends sensitively on both its intrinsic stability and the growth environment. CdS has two common crystal structures—hexagonal and cubic—with the former being thermodynamically favored. For hexagonal CdS, the polar axis along the [001] direction is the preferred growth orientation, whereas cubic CdS grows preferentially along the [111] direction.[42,43] It should be noted that one hexagonal cell consists of at least two layers of CdS_4 tetrahedra stacked along the [001] direction, and at least four tetrahedral layers are needed along the [111] direction to constitute one cubic cell. Furthermore, the binding energy of cubic CdS is lower than that of hexagonal CdS so that the cubic phase is not thermodynamically favored. In our synthesis, it is likely that variations in the crystalline phase result from differences in the symmetry of the first coordination sphere of Cd with S in the thioacetamide complex and the corresponding growth conditions. Lower symmetry of the complex, in a low sulfur/cadmium molar ratio solution, favors formation of the cubic symmetry and their growth along the [111] direction. In contrast, formation of CdS with the thermodynamically more stable hexagonal structure is favored for higher sulfur/cadmium molar ratios. During the initial stage, crystal nuclei may develop into seeds with the preferred form, especially under nonequilibrium conditions. However, during the subsequent stage, external conditions can influence the ability of tetrahedral growth units of the seeds with different facets to coalesce.

We have tested the *E. coli*-templated nanoporous hollow CdS microrods as photocatalyst for hydrogen production. To investigate their photocatalytic activity, the as-synthesized material with the hexagonal crystal structure is deposited in the form of a coating on ITO-coated glass substrate and annealed at 300 °C for 0.5 h. We have confirmed that the hollow microrod structure is retained after the annealing process (Figure 8). The photoelectrochemical properties of the fabricated CdS photoanodes are then measured in 1 M Na_2S/0.5 M $NaSO_3$ electrolyte

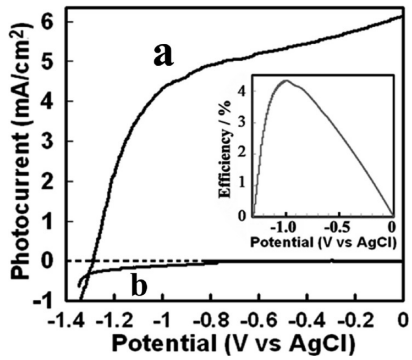

Figure 9. (a) Photocurrent density, (b) dark current, and corresponding photoconversion efficiency (the inset) of a photoelectrode fabricated using *E. coli*-templated nanoporous CdS hollow microrods with the hexagonal phase structure.

under global AM 1.5 illumination with conventional three-electrode system consisting of a Ag/AgCl reference electrode and a Pt foil counter electrode. From these measurements, the photoconversion efficiency of light energy to chemical energy is calculated by using the photoelectrochemical cell efficiency, as has been reported previously.[38,39] A photoconversion efficiency of 4.3% is obtained, as shown in Figure 9. This value is much higher than the 1.2% efficiency obtained using CdS nanoparticles synthesized using the same procedure in the absence of *E. coli*. In our experiments, about 15% of the incident light is reflected by the reactor wall and adsorbed by the reaction solution. In addition, the photoelectrochemical cell efficiency values vary depending upon the errors and deviation involved in the assumptions and measurement procedures, such as the instruments' measuring deviation, the mismatch between the actual spectrum, and the actual spectrum at the time of measurement, etc. As for the instruments and the measurement procedure used in the present work, a duplicate experiment showed good reproducibility for the photoelectrochemical cell efficiency measurement and a standard deviation of less than 7% for five repetitive measurements.

The enhanced photoconversion efficiency in the case of the CdS microrods is attributed to both enhanced light absorption and fast electron transport due to the porous structure and thin rod wall thickness. Electron transport and electron/hole recombination are critical issues for bulk materials in photocatalytic applications. Nanopores in the hollow CdS microrods provide an ideal pathway for electron transport so that ejected electrons can be transported rapidly to reduce recombination. This is similar to the transport process reported in CdS-coated TiO_2 nanotube array photoelectrodes in which photoexcited electrons can rapidly migrate to the TiO_2 nanotubes, thereby decreasing the electron−hole recombination.[38]

The likely reaction mechanism for photocatalytic hydrogen production over CdS in the presence of S^{2-} and SO_3^{2-} has been described previously.[10] Briefly, when a photon is absorbed by CdS on the photoanode in the presence of S^{2-} and SO_3^{2-}, an electron/hole (e^-/h^+) pair is generated. The h^+ can oxidize the adsorbed SO_3^{2-} and S^{2-} on the surface of the photoanode to form SO_4^{2-} and S_2^{2}, while the e^- migrates to the Pt counter electrode and reduces water to form H_2.

The simple synthetic strategy of using ethanol treated *E. coli* as template has been extended to the preparation of other sulfide nanostructures, including PbS, HgS, and ZnS, as seen in Figure 10. We are in the process of fabricating and characterizing some mixed chalcogenide nanostructures and investigating their photoconversion efficiency.

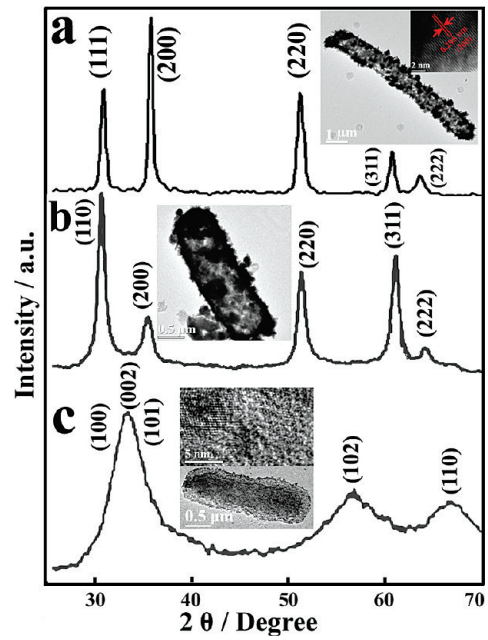

Figure 10. XRD patterns and TEM images of *E. coli*-templated nanoporous hollow microrods of (a) PbS, (b) HgS, and (c) ZnS sonochemically synthesized after 4 h of reaction.

Conclusion

In summary, we have used ethanol-treated *E. coli* bacteria as a template to promote controllable growth of nanoporous hollow CdS microrods via a simple sonochemical synthetic method. The crystal phase, morphology, micro-/nanostructure, optical absorption, and photocatalytic properties of the CdS nanomaterials have been tailored over a wide range by simply changing the synthetic conditions, including the sulfur/cadmium molar ratio of the reactants, the reaction time, and the growth condition of *E. coli* bacteria. A significant improvement in the photoconversion efficiency has been achieved utilizing the unique nanoporous hollow structures resulting from effective kinetic separation of the photogenerated carriers. The facile synthesis procedure can be extended to the fabrication of other sulfides and core−shell nanostructures that will potentially lead to further improvements in the photoconversion efficiency. Controlled growth of semiconductor nanorod antennas utilizing the *E. coli* pili provides another avenue for increased efficiency by aiding in the energy harvesting process.

Acknowledgment. Research supported by the U.S. Department of Energy, Office of Basic Energy Sciences, Division of Materials Sciences and Engineering under Award # DE-FG02-08ER46537.

References and Notes

(1) Zong, X.; Yan, H.; Wu, G.; Ma, G.; Wen, F.; Wang, L.; Li, C. *J. Am. Chem. Soc.* **2008**, *130*, 7176.
(2) Tsuji, I.; Kato, H.; Kudo, A. *Angew. Chem., Int. Ed.* **2005**, *44*, 3565.
(3) Tsuji, I.; Kato, H.; Kobayashi, H.; Kudo, A. *J. Am. Chem. Soc.* **2004**, *126*, 13406.
(4) Nanu, M.; Schoonman, J.; Goossens, A. *Nano Lett.* **2005**, *5*, 1716.
(5) Matsumura, M.; Saho, Y.; Tsubomura, H. *J. Phys. Chem.* **1983**, *87*, 3807.
(6) Bao, N.; Shen, L.; Takata, T.; Domen, K.; Gupta, A.; Yanagisawa, K.; Grimes, A. C. *J. Phys. Chem. C* **2007**, *111*, 17527.
(7) Kudo, A.; Kato, H.; Tsuji, I. *Chem. Lett.* **2004**, *33*, 1534.
(8) Arai, T.; Senda, S.; Sato, Y.; Takahashi, H.; Shinoda, K.; Jeyadevan, B.; Tohji, K. *Chem. Mater.* **2008**, *20*, 1997.

(9) Zheng, N.; Bu, X.; Vu, H.; Feng, P. *Angew. Chem., Int. Ed.* **2005**, *44*, 5299.
(10) Bao, N.; Shen, L.; Takata, T.; Domen, K. *Chem. Mater.* **2008**, *20*, 110.
(11) Agrawal, M.; Pich, A.; Zafeiropoulos, N. E.; Gupta, S.; Pionteck, J.; Simon, F.; Stamm, M. *Chem. Mater.* **2007**, *19*, 1845.
(12) Chen, M.; Wu, L. M.; Zhou, S. X.; You, B. *Adv. Mater.* **2006**, *18*, 801.
(13) Wang, Y.; Wang, G.; Wang, H.; Cai, W.; Zhang, L. *Chem. Commun.* **2008**, 6555.
(14) Du, N.; Zhang, H.; Chen, J.; Sun, J.; Chen, B.; Yang, D. *J. Phys. Chem. B* **2008**, *112*, 14836.
(15) Ahmad, J.; Dickerson, M. B.; Cai, Y.; Jones, S. E.; Ernst, E. M.; Vernon, J. P.; Haluska, M. S.; Fang, Y.; Wang, J.; Subramanyam, G.; Naik, R. R.; Sandhage, K. H. *J. Am. Chem. Soc.* **2008**, *130*, 4.
(16) Kisailus, D.; Truong, Q.; Amemiya, Y.; Weaver, J. C.; Morse, D. E. *Proc. Natl. Acad. Sci. U.S.A.* **2006**, *103*, 5652.
(17) Ma, N.; Dooley, C. J.; Kelley, S. O. *J. Am. Chem. Soc.* **2006**, *128*, 12598.
(18) Sharma, J.; Chhabra, R.; Andersen, C. S.; Gothelf, K. V.; Yan, H.; Liu, Y. *J. Am. Chem. Soc.* **2008**, *130*, 7820.
(19) Whaley, S. R.; English, D. S.; Hu, E. L.; Barbara, P. F.; Belcher, A. M. *Nature* **2000**, *405*, 665.
(20) Prozorov, T.; Palo, P.; Wang, L.; Nilsen-Hamilton, M.; Jones, D.; Orr, D.; Mallapragada, S. K.; Narasimhan, B.; Canfield, P. C.; Prozorov, R. *ACS Nano* **2007**, *1*, 228.
(21) Sanchez, C.; Arribart, H.; Guille, M. M. G. *Nat. Mater.* **2005**, *4*, 277.
(22) Niemeyer, C. M. *Angew. Chem., Int. Ed.* **2001**, *40*, 4128.
(23) Zhang, S. *Nat. Biotechnol.* **2003**, *21*, 1171.
(24) Douglas, T.; Young, M. *Adv. Mater.* **1999**, *11*, 679.
(25) Yoo, P. J.; Nam, K. T.; Qi, J.; Lee, S. K.; Park, J.; Belcher, A. M.; Hammond, P. T. *Nat. Mater.* **2006**, *5*, 234.
(26) Nam, K. T.; Kim, D.; Yoo, P. J.; Chiang, C.; Meethong, N.; Hammond, P. T.; Chiang, Y.; Belcher, A. M. *Science* **2006**, *312*, 885.
(27) Nam, K. T.; Wartena, R.; Yoo, P. J.; Liau, F. W.; Lee, Y. J.; Chiang, Y.; Hammond, P. T.; Belcher, A. M. *Proc. Natl. Acad. Sci. U.S.A.* **2008**, *105*, 17227.
(28) Vriezema, D. M.; Aragones, M. C.; Elemans, J. A. A. W.; Cornelissen, J. J. L. M.; Rowan, A. E.; Nolte, R. J. M. *Chem. Rev.* **2005**, *105*, 1445.
(29) Mandal, D.; Bolander, M. E.; Mukhopadhyay, D.; Sarkar, G.; Mukherjee, P. *Appl. Microbiol. Biotechnol.* **2006**, *69*, 485.
(30) Levinson, W. *Review of Medical Microbiology & Immunology*, 10th ed.; McGraw-Hill Companies, Inc.: New York, 2008.
(31) Sweeney, R. Y.; Mao, C.; Gao, X.; Burt, L. L.; Belcher, A. M.; Georgiou, G.; Iverson, B. L. *Chem. Biol.* **2004**, *11*, 1553.
(32) Kang, S. H.; Bozhilov, K. N.; Myung, N. V.; Mulchandani, A.; Chen, W. *Angew. Chem., Int. Ed.* **2008**, *120*, 5264.
(33) Mehra, R. K.; Winge, D. R. *J. Cell. Biochem.* **1991**, *45*, 30.
(34) Vido, K.; Spector, D.; Lagniel, G.; Lopez, S.; Toledano, M. B.; Labarre, J. *J. Biol. Chem.* **2001**, *276*, 8469.
(35) Zhou, H.; Fan, T.; Zhang, D.; Guo, D.; Ogawa, H. *Chem. Mater.* **2007**, *19*, 2144.
(36) Cassler, M. R.; Grimwade, J. E.; McGarry, K. C.; Mott, R. T.; Leonard, A. C. *Nucleic Acids Res.* **1999**, *27*, 4570.
(37) Dhas, N. A.; Zaban, A.; Gedanken, A. *Chem. Mater.* **1999**, *11*, 806.
(38) Sun, W. T.; Yuan, Y.; Pan, H. Y.; Gao, X. F.; Chen, Q.; Peng, L. M. *J. Am. Chem. Soc.* **2008**, *130*, 1124.
(39) Tak, Y.; Hong, S.; J. Lee, J. S.; Yong, K. *J. Mater. Chem.* **2009**, *19*, 5945.
(40) Beard, J.; Howe, T.; Richmond, M. *J. Bacteriol.* **1972**, *111*, 814.
(41) Gao, T.; Li, Q.; Wang, T. *Chem. Mater.* **2005**, *17*, 887.
(42) Yong, K.; Sahoo, Y.; Swihart, M. T.; Prasad, P. N. *J. Phys. Chem. C* **2007**, *111*, 2447.
(43) Chen, M.; Kim, Y. N.; Li, C.; Cho, S. *Cryst. Growth Des.* **2008**, *8*, 629.

JP910842F